Journal of Chemical Health Risks

ORIGINAL ARTICLE

Modified Titania Impact on Photocatalytic Efficiency of Bmim [Cl]

Aina Farwizah Shahhiran, Raihan Mahirah Ramli[*], Hayyiratul Fatimah Mohd Zaid

Department of Chemical Engineering, Universiti Teknologi PETRONAS, Bandar Seri Iskandar, 32610, Perak, Malaysia

ABSTRACT: Titania has been one of the promising alternatives in treating environmental pollution issues and was considered in various applications due to its flexible behaviour. Many studies have been conducted to test its phase-changing properties and adaptive ability such as calcination process, and metal and nonmetal modification using mono-doped or co-doped elements. In the present study, the photocatalyst was developed from embedment with activated carbon (AC) followed by co-doping of Cu^{2+} and Fe^{3+} metal ions. The photocatalyst was characterized by XRD, BET and FESEM. The synthesized photocatalyst was tested in the photocatalytic degradation system for ionic liquid (IL) at the optimized parameters which includes solution pH = 6, [photocatalyst] = 1 g L^{-1} and [H_2O_2] = 0.75 ml L^{-1}. The co-doped product exhibited a smaller crystalline sizes as compared to bare TiO_2. In addition, copper and iron dopants are well dispersed into the TiO_2 lattice as no additional phases were detected. Maximum degradation of 77% of 0.11mM IL was recorded in the Cu:Fe-TiO_2/AC system after 240 min of visible light irradiation. The system's efficiency in terms of tested photocatalysts is in the order of P25 < TiO_2 < TiO_2/AC < Cu:Fe-TiO_2/AC, respectively.

INTRODUCTION

The booming applications of ionic liquids (ILs) in industry is owing to their tuneable properties to meet specific demand [1]. Their negligible vapour pressure makes them a better alternative solvent for various application. Yet, their high in-water solubility and stability leads to another environmental issue of water pollution. Low biodegradability of ILs was reported in several studies [2, 3] which would cause adverse effect to the aquatic system.

Among those common wastewater treatment processes used in industry[4] and research[5], advanced oxidation processes (AOPs) have been widely reported for degradation of wide range of organic pollutants due to their high efficiency[6]. In depth studies has been conducted on AOPs utilizing photocatalysts for refinement of treated water and air. The efficiency of this process has been proven in its ability to remove impurities and pollutants with the used of semiconductor catalyst and UV- or visible light-assisted without additional oxidizing agent[7]. One of the widely reported AOPs is photocatalytic degradation system employing semiconductor titanium dioxide (TiO_2) as photocatalyst to harvest light energy to officiate chemical reaction[8,9]. This semiconductor has gained interest recently due to its attractive properties such as chemical and biological stability, cheap availability, low toxicity, environmental friendly and high photocatalytic activity[10].

In particular, TiO_2 with predominantly anatase phase can be used as photocatalyst under UV illumination. The photocatalytic reaction starts with the UV light absorption about similar or higher energy than the band gap energy as of anatase TiO_2 (around 389 nm or lower). These phenomenon results in the excitation of electrons in the valence band ($e_{cb}^{\square}$) and triggers the formation of

positive holes (h_{vb}^+). In addition, these electrons can react with oxygen while the positive holes can react with hydroxyl ion (^-OH) and water molecules (H_2O) on the surface of TiO_2 to generate radicals. These free radicals are sufficiently strong to oxidize and decompose numerous organic materials into harmless transition products such as CO_2 and H_2O consecutively until the system reaching the new equilibrium [11].

Despite of the capability of TiO_2, there are still several drawbacks of the photocatalyst such as the difficulty to recycle as it is easy to agglomerate, high electron-hole recombination rate and wide band gap energy which makes it less efficient in removing those organic compounds. A few articles have reported an improved bare TiO_2 performance when shifted into visible light region of solar spectrum which accounts for *ca.* 42% on the sunlight. One of the modification methods of TiO_2 is by doping transition metals such as Cu, Cr, Fe, Mo and W[12]. The presence of these metals on the TiO_2 contributes to the additions of active sites which results in higher photocatalytic degradation efficiency[13].

A study conducted on bmim[Cl] photodegradation utilizing Fe-TiO_2 catalyst manage to achieve a mineralization up to 36% by adjusting a few intrinsic factors within the system[14]. Same goes to Cu-TiO_2 catalyst with 58% removal of Azo dyes contaminant[15]. However, a slightly higher degradation percentage can be achieved from the co-doping of TiO_2 catalyst[16] which in line to several studies reported where the incorporation of two types cations into TiO_2 lattice has enhanced the photoactivity of titania due to cooperative effects of both dopants. Momeni and Ghayeb has compared the efficiency of photocatalytic activity between unmodified TiO_2, single doped metal-TiO_2 as well as co-doped metal–TiO_2. Results show that co-doped metal–TiO_2 samples exhibited higher photocatalytic activity in the degradation of organic pollutant. Kinetic study also displays the reaction rate constant of co-doped metal–TiO_2 with approximately 2.26 times higher than the apparent reaction rate constant of bare single doped metal–TiO_2 [17].

Thus, the aim of this research paper is to investigate the performance of modified bimetallic TiO_2 with Cu and Fe for visible light degradation of ionic liquid specified to 1-butyl-3-methylimidazolium chloride (bmim[Cl]). The work analysed the ability of serial modification conducted on bare TiO_2 photocatalysts to obtain a deeper insight on the efficiency of each catalyst in degrading bmim[Cl].

MATERIALS AND METHODS

Heptane, Triton X-100, Hexanol, Titanium isopropoxide (TTIP), Iron (II) nitrate ($Fe(NO_3)_2 \cdot 9H_2O$), Copper (II) chloride ($CuCl_2.2H_2O$), 1-butyl-3-methylimidazolium chloride (bmim[Cl]), Methanol (CH_3OH, 99.8%), Phosphoric acid (H_3PO_4, 85%), Potassium dihydrogen phosphate (KH_2PO_4) and Triethylamine ($C_6H_{15}N$, AR) were purchased from Merck (Darmstadt, Germany). Deionised water was used in all experimental procedures.

Synthesis of photocatalyst

TiO_2 was synthesized by following the method reported elsewhere[15]. The resulting white powder was doped with Cu and Fe via wetness impregnation method by adding the metal precursor at predetermined amount of dopant (0.2 wt% total metal loading with 1Cu:2Fe ratio) into the TiO_2 suspended solution. In another set-up, biochar was treated in a boiled 1 M nitric acid solution for 20 mins and was then rinsed with deionised water repeatedly until a neutral supernatant was produced. The solid residue was dried overnight at 105^0 C to produce activated carbon (AC). The Cu:Fe-TiO_2 prepared in previous step was mixed with appropriate amount of AC through impregnation method for the formation of desired photocatalysts. The resultant solid product was then calcined in a muffle furnace at 400ºC for 1.5 h duration and allowed to cool until it reaches room temperature. Finally, the granule was crushed using pestle mortar till a fine powder can be collected as the end-product.

Characterization of modified photocatalyst

The phase existence and crystallinity of the prepared photocatalysts was determined using Bruker D8 Advanced XRD with Cu Kα radiation (40 kV, 40 mA) at 2θ angles from 10° to 90°, with a scan speed of 4° min^{-1}. The dominant peak of anatase (2θ = 25.7º) was used to estimate the crystallite sizes by using Scherrer equation[18].

BET analysis was used to measure the specific surface area and pore volume of the photocatalyst as these are important properties in photocatalytic process. TriStar II 3020 surface area analyzer was used to quantify the surface area.

The morphological structure and related properties of selected photocatalysts were observed using FESEM Model Zeiss Supra 35VP equipped with EDX. The analysis was conducted using 10kV EHT, with magnification between 50 to 150 kX and working distance between of 3 to 5 mm.

Photodegradation study

Photocatalytic degradation process was conducted in an open glass reactor based on the parameters which was already being reported in previous work[16]. In a typical photodegradation study, 100 mL of IL solution was placed in the reactor with predetermined amount of photocatalyst to produce suspended solution under constant stirring. The system was stirred in the absent of light for 30 mins to reach adsorption-desorption equilibrium. Then, H_2O_2 was added and the 500 W halogen lamp was switched on to simulate for visible light radiation to allow for photodegradation process to occur. The photodegradation process was conducted for 4 h duration.

Residual concentration of the samples was measured every 1 h. Samples were taken at regular time intervals and filtered using 0.45μm syringe filter to remove the photocatalyst residue. Then, the absorbance was quantified by using HPLC at 212 nm on Agilent 1100 instrument equipped with UV detector. A symmetry C-18 column (5 μm, 250 mm, 4.6 mm) as stationary phase and phosphate buffer containing a mixture of methanol (35 vol %) and 0.5% of triethylamine were used for a better separation and sharp analysis. The total IL removal was calculated based on initial and final residual concentrations to determine the efficiency of the tested photocatalyst.

RESULTS AND DISCUSSION

X-ray Diffraction (XRD)

The XRD patterns of Degussa P25 (used as standard), pristine TiO_2, TiO_2/AC and $Cu:Fe-TiO_2/AC$ composites are shown in Figure 1. All photocatalysts are well crystallize. Major peaks for Degussa-P25 was detected around 25.5° (101) and 48.3° (110) which indicates the anatase phases but the rutile peak could still be visibly seen. It is a well-established data that the commercial bicrystalline TiO_2 consists of both anatase and rutile phase[15]. Meanwhile for the pristine TiO_2, there is no presence of rutile phase in comparison to the P25. Pure phases is generally accepted as anatase exhibits a higher photocatalytic activity compared to rutile TiO_2 [19]. The peaks recorded at 25.7° (101), 38.1° (004), 48.4° (200), 54.14 (105), 63.0° (204) represent anatase phase of TiO_2. There is no additional peak recorded for AC and metal ions after they deposited onto TiO_2 which indicates a well dispersion of these entities into TiO_2 lattice[14,20].
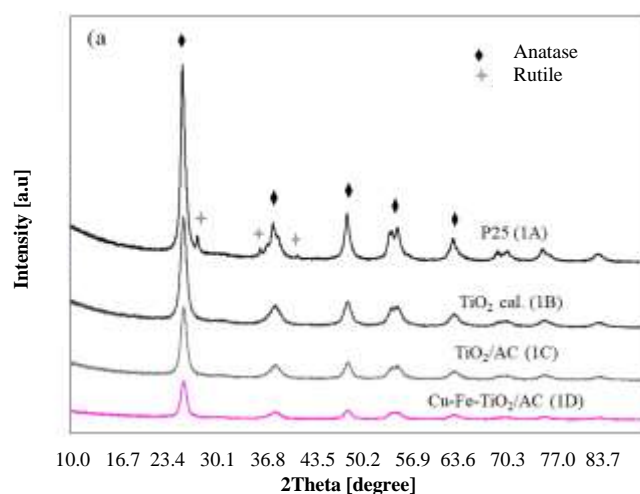
Figure 1. The XRD diffraction spectra: (a) XRD pictogram for Degussa P25, pristine TiO_2, TiO_2/AC and $Cu:Fe-TiO_2/AC$, (b) Comparison of the XRD anatase (101) plane peaks and (c) anatase (200) plane peaks.
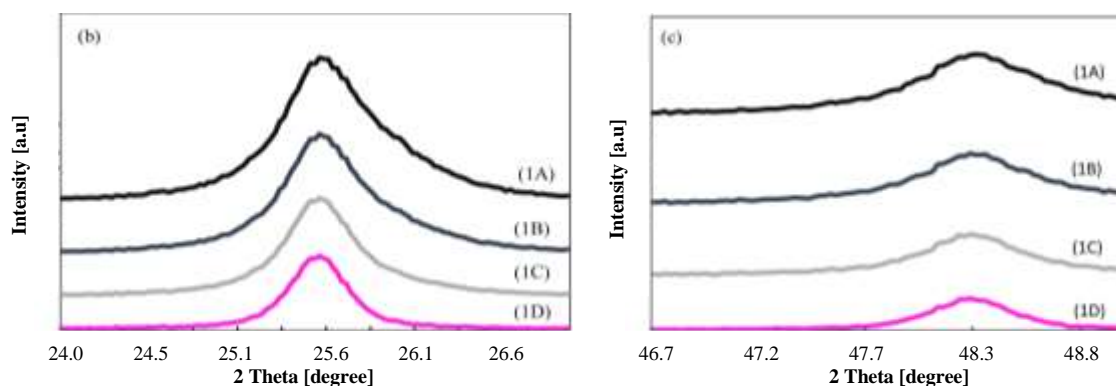
Figure 1. Continued

In comparison of the anatase peak at plane 101 (25.7⁰), P25 has the highest peak while Cu:Fe-TiO$_2$/AC has the lowest. The pristine TiO$_2$ has smaller crystallite size (10.2 nm) compared to P25, while other photocatalysts have comparable size (Table 1). Although all photocatalysts have undergone stages of heat treatment process, the crystallite sizes are smaller than the standard P25, and also similar to pristine TiO$_2$. In general, heat treatment applied to TiO$_2$ during the calcination stages will promote the growth of particles and the formation of rutile phases. However, the effect was negligible for the composite photocatalyst which could be attributed to the presence of AC and also bimetallic element[21]. This observation shows that, the presence of AC (contains interfacial energy) as a support and also Cu:Fe as the metal dopants could suppress the growth of TiO$_2$ and

reduce the agglomeration effect during the synthesis process, thus providing well-define structure (Figure 2.) with small particle size[20,21,22]. The XRD spectra for (101) and (201) anatase peaks scanned P25, TiO$_2$ and modified TiO$_2$ nanomaterials are illustrated in Figure 1(b) and 1(c). A broadening of the major anatase peaks (101) and (201) can be detected which implies a decrease in crystalline size prior to additional dopant component[23]. The crystallographic constant and particle size of photocatalyst are tabulated in Table 1. where a slight change in crystallographic constant indicates the occurrence of lattice distortion to enhance the surface modification. The distortion occurred due to the incorporation of both Cu^{2+} and Fe^{3+} into the TiO$_2$ lattice hence affecting the crystallographic constant of TiO$_2$ [24].

Table 1. Crystallographic constant and particle size of photocatalyst.

Photocatalyst	Crystallographic Constant (Å)			Crystallite size (nm)
	a	b	c	
P25	-	-	-	21
TiO$_2$	3.776	3.776	9.486	10.2
TiO$_2$/AC	3.777	3.777	9.501	10.0
Cu:Fe-TiO$_2$/AC	3.771	3.771	9.430	10.2

Surface Area and Porosity (BET)

The porosity data of photocatalysts are presented in Table 2. From the table, TiO$_2$/AC has the highest surface area which significantly verify the existence of AC [25] while the smallest surface area is recorded for P25 [26]. The increment of the surface area for the composite photocatalysts as compared to P25 and even pristine TiO$_2$ is due to the presence of AC, with the addition of Cu:Fe which could further suppress the growth of TiO$_2$ and reduce the agglomeration rate during the synthesis

process, thus providing smaller particle size. There is direct correlation between the particle size and surface area, where the smaller the particle size, the higher the surface area. From the data, it can be observed that smaller particles produce larger surface area. High surface area is generally favoured in photocatalytic degradation system due to more active sites available for formation of oxidant species that is responsible to degrade the pollutant.

Table 2. Porosity properties TiO_2, $TiO_2/10AC$ and $Cu:Fe-TiO_2/10AC$.

Photocatalyst	$S_{BET}(m^2 g^{-1})$	$V_{total} (cm^3 g^{-1})$	Pore diameter (nm)
P25	56	0.25	17.5
TiO_2	100.53	0.26	10.13
TiO_2/AC	111.97	0.20	7.28
$Cu:Fe-TiO_2/AC$	104.03	0.22	8.22

Field Emission-Scanning Electron Microscopic (FESEM)

The morphological structure of pristine TiO_2, TiO_2/AC and $Cu:Fe-TiO_2/AC$ are depicted in Figure 2. The pristine TiO_2 in Figure 2(a) shows nano-spherical and uniform structure, similar to P25 morphological structure reported[27] but with much smaller particles observed. This is due to the synthesis method through microemulsion process where the particles size could be controlled within the nanoreactor formed during the synthesis step. Comparing to the pristine TiO_2 and the TiO_2/AC (Figure 2(b), the latter shows a different structure with less degree of agglomeration (the first is much denser particles). This could be due to high porosity structure of AC [28] causing high dispersion of TiO_2 onto the AC support thus supressing the agglomeration rate during the calcination process[29, 30].

On the other hand, the $Cu:Fe-TiO_2/AC$ in Figure 2(c) shows a well-defined and ordered nanoparticle structure with less degree of agglomeration. Generally, the incorporation of Cu and Fe into TiO_2 lattice could suppress the growth of TiO_2 during the calcination process thus produce smaller particle size with high surface area which is in line with the data obtained from XRD and BET analysis. The incorporation of Fe would contribute to the suppression growth rate of TiO_2 into very fine particle structure [31] while Cu presence is able to enhance the crystalline structure of TiO_2 [32]. This is agreeable to a study stating that co-doping does increase the surface area and decreased the crystallinity of a semiconductor. This alteration in lattice parameters results in structural distortion as the doping species were successfully incorporated into TiO_2 lattice [33].
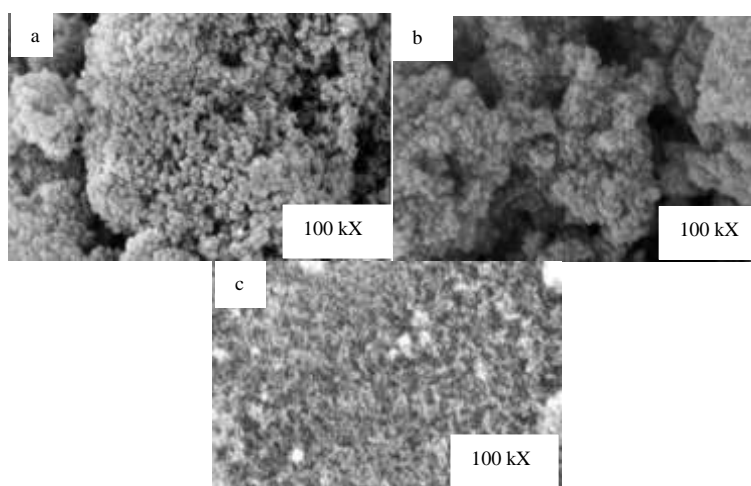
Figure 2. FESEM micrograph for (a) TiO_2, (b) TiO_2/AC, and (c) $Cu:Fe-TiO_2/AC$.

Photodegradation study

Figure 3 compares the efficiency of the photocatalytic degradation system of bmim[Cl] containing different photocatalyst. P25 was used as the standard for comparison. The lowest removal of bmim[Cl] is recorded from P25 system, while only slight improvement could be obtained when using the pristine TiO_2. These performances are as expected due to the low ability of

both photocatalysts to harvest visible light energy to stimulate the chemical reaction within the system. TiO_2 could only absorb light energy of below 390 nm while visible light region is beyond 400 nm. An increment of *ca.* 6% removal could be attributed to the presence of AC in the composite photocatalyst which enhance the adsorption of bmim[Cl] onto the photocatalyst surface

due to the synergistic effect of adsorption-photodegradation of TiO_2/AC. However, similar to previous systems, the efficiency of light harvesting components is low due to the limitation of the TiO_2.
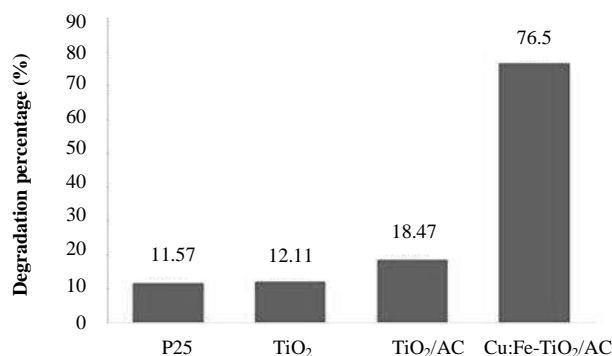
Figure 3. Degradation of bmim[Cl] utilizing P25, pristine TiO_2, TiO_2/AC and Cu:Fe-TiO_2/AC

Further modification with Cu and Fe recorded a drastic increment of the system's efficiency near to 80% total removal (Figure 3). It can be observed that the doping of semiconductor metals onto the TiO_2 lattice have contribute to a tremendous effect on bmim[Cl] degradation. This may be due to the combination of Cu:Fe metal ions which suppress the growth of TiO_2 during synthesis process where pure anatase structure had been produce with smaller particles size as shown in XRD analysis. Smaller particle size could provide higher surface area as displayed in BET analysis which could improve the adsorption of bmim[Cl] on photocatalysts surface, thus enhance the diffusion rate of bmim[Cl] on TiO_2 surface[34].

Increasing the surface area of a catalyst exposes more ionic liquid molecules to be attack as more active sites were provided for the process to take place. The introduction of Cu and Fe metal ions also give rise to the formation of a space charge layer which consequently reduced the recombination rate of electron hole ($e_{cb}^{\square}$ - h_{vb}^{+}) pairs by becoming the trapping site for electron. Hence, the free h_{vb}^{+} are able to participate in the reaction within the system assisted by the presence of O-H groups on the composite photocatalyst which act as the pollutant concentrator and enhanced the conductivity of tested photocatalyst. This synergistic effect of adsorption-photodegradation significantly improved the overall efficiency of the system[10].

CONCLUSIONS

The incorporation of Cu and Fe into TiO_2/AC has significantly increased the synergistic effect of adsorption-desorption of the composite photocatalyst. The system recorded of 77% removal efficiency; 4 folds higher than the system without metal dopants. Optimization of the system's operating variables could be further conducted to improve the efficiency near to completion of total removal. The system's efficiency is in the order of P25 < TiO_2 < TiO_2/AC < Cu:Fe-TiO_2/AC, respectively.

Conflict of interests

No coflict.

REFERENCES

1. Siedlecka E.M., Czerwicka M., Neumann J., Stepnowski P., Fernndez J.F., Thöming J., 2011. Ionic Liquids: Methods of Degradation and Recovery. Ionic Liquids: Theory, Properties, New Approaches.

2. Romero A., Santos A., Tojo J., Rodríguez A., 2008. Toxicity And Biodegradability of Imidazolium Ionic

Liquids. Journal of Hazardous Materials. 151(1), 268-273.

3. Maria Siedlecka E., Czerwicka M., Stolte S., Stepnowski P., 2011. Stability of Ionic Liquids In Application Conditions. Current Organic Chemistry. 15(12), 1974-1991.

4.Tekin H., Bilkay O., Ataberk S.S., Balta T.H., Ceribasi I.H., Sanin F.D., Dilek F.B., Yetis U., 2006. Use of Fenton Oxidation To Improve The Biodegradability Of A Pharmaceutical Wastewater. Journal of Hazardous Materials. 136(2), 258-265.

5. Aljuboury D.A.A, Palaniandy P., Abdul Aziz H., Feroz S., 2017. Evaluation of The Photocatalyst of TiO_2/Fenton/ZnO To Treat The Petroleum Wastewater of the International Conference of Global Network for Innovative Technology and AWAM International Conference in Civil Engineering, August 8-10, 19, pp. 439-452.

6. Czerwicka M., Stolte S., Müller A., Siedlecka E., Gołębiowski M., Kumirska J., Stepnowski P., 2009. Identification Of Ionic Liquid Breakdown Products In An Advanced Oxidation System. Journal of Hazardous Materials. 171, 478-483.

7. Yoon J.W., Baek M.H., Hong J.S., Lee C.Y., Suh J.K., 2012. Photocatalytic Degradation of Azo Dye Using TiO_2 Supported on Spherical Activated Carbon. Korean Journal of Chemical Engineering. 29(12), 1722-1729.

8. Haarstrick A., Kut O.M., Heinzle E., 1996. TiO_2-Assisted Degradation of Environmentally Relevant Organic Compounds In Wastewater Using a Novel Fluidized Bed Photoreactor. Environmental Science & Technology. 30(3), 817-824.

9. Lachheb H., Puzenat E., Houas A., Ksibi M., Elaloui E., Guillard C., Herrmann J.M., 2002. Photocatalytic Degradation of Various Types of Dyes (Alizarin S, Crocein Orange G, Methyl Red, Congo Red, Methylene Blue) In Water By UV-Irradiated Titania. Applied Catalysis B: Environmental. 39(1), 75-90.

10. El-Salamony R., Amdeha E., Ghoneim S.A., Badawy N.A., Salem K.M., Al-Sabagh A.M., 2017. Titania Modified Activated Carbon Prepared From Sugarcane Bagasse: Adsorption And Photocatalytic Degradation Of Methylene Blue Under Visible Light Irradiation. Environmental Technology. 38(24), 3122-3136.

11.Yap P.S., Lim T.T., 2012. Solar Regeneration of Powdered Activated Carbon Impregnated With Visible-Light Responsive Photocatalyst: Factors Affecting Performances And Predictive Model. Water Research. 46(9), 3054-3064.

12. Paola A.D., Ikeda S., Marcì G., Ohtani B., Palmisano L., 2001. Transition Metal Doped TiO_2: Physical Properties And Photocatalytic Behaviour. International Journal of Photoenergy. 3(4), 171-176.

13.Kumar S.G., Devi L.G., 2011. Review on Modified TiO_2photocatalysis Under UV/Visible Light: Selected Results And Related Mechanisms On Interfacial Charge Carrier Transfer Dynamics. The Journal of Physical Chemistry A. 115(46), 13211-13241.

14. Zawawi A., Ramli R.M., Yub Harun N., 2017. Photodegradation of 1-Butyl-3-Methylimidazolium Chloride [Bmim]Cl Via Synergistic Effect of Adsorption–Photodegradation of Fe-TiO_2/AC. Technologies. 5(4), 82.

15. Ramli R.M., Chong F.K., Omar A.A., Murugesan T., 2014. Performance of Surfactant Assisted Synthesis of Fe/Tio2on The Photodegradation of Diisopropanolamine. CLEAN - Soil, Air, Water. 43(5), 690-697.

16. Farwizah Shahhiran A., Ramli R.M., Mohd Zaid H.F., 2020. Development of Photocatalytic Degradation And Kinetic Study For Imidazolium Based Ionic Liquids In Fe-Cu/TiO_2-AC System. IOP Conference Series: Earth and Environmental Science. 442, 012001.

17. Momeni M.M., Ghayeb Y., 2016. Preparation of Cobalt Coated TiO_2 and WO_3 –TiO_2 Nanotube Films Via Photo-Assisted Deposition With Enhanced Photocatalytic Activity Under Visible Light Illumination. Ceramics International. 42(6), 7014-7022.

18. Hwang K.J., Lee J.W, Shim W.G., Jang H.D., Lee S.I., Yoo S.J., 2012. Adsorption And Photocatalysis Of Nanocrystalline TiO_2 Particles Prepared By Sol–

Gel Method For Methylene Blue Degradation. Advanced Powder Technology. 23(3), 414-418.

19. Luttrell T., Halpegamage S., Tao J., Kramer A., Sutter E., Batzill M., 2014. Why Is Anatase A Better Photocatalyst Than Rutile? - Model Studies on Epitaxial Tio2 Films. Scientific Reports. 4(1), 4043.

20. Asiltürk M., Sayılkan F., Arpaç E., 2009. Effect of Fe^{3+} Ion Doping To TiO_2 On The Photocatalytic Degradation of Malachite Green Dye Under UV And Vis-Irradiation. Journal of Photochemistry and Photobiology A: Chemistry. 203(1), 64-71.

21. Wang X., Hu Z., Chen Y., Zhao G., Liu Y., Wen Z., 2009. A Novel Approach Towards High-Performance Composite Photocatalyst of TiO_2 Deposited On Activated Carbon. Applied Surface Science. 255(7), 3953-3958.

22. Naeem K., Ouyang F., 2010. Preparation of Fe^{3+}-Doped TiO_2 Nanoparticles And Its Photocatalytic Activity Under UV Light. Physica B: Condensed Matter. 405(1), 221-226.

23. Sahu, M., Biswas, P., 2011. Single-Step Processing of Copper-Doped Titania Nanomaterials In A Flame Aerosol Reactor. Nanoscale Research Letters. 6(1), 1-14.

24. Ramli R.M., Kait C.K., Omar A.A., 2016. Remediation of DIPA Contaminated Wastewater Using Visible Light Active Bimetallic Cu-Fe/TiO_2 Photocatalyst. Procedia Engineering. 148, 508-515.

25. Khalid N.R., Ahmed E., Hong Z., Ahmad M., Zhang Y., Khalid S., 2013. Cu-Doped TiO_2 Nanoparticles/Graphene Composites For Efficient Visible-Light Photocatalysis. Ceramics International. 39(6), 7107-7113.

26. Gao B., Yap P.S., Lim T.M., Lim T.T., 2011. Adsorption-Photocatalytic Degradation Of Acid Red 88 By Supported Tio2: Effect Of Activated Carbon Support And Aqueous Anions. Chemical Engineering Journal. 171(3), 1098-1107.

27. Raj K.J.A., Viswanathan B., 2009. Effect of Surface Area, Pore Volume and Particle Size of P25 Titania On The Phase Transformation Of Anatase To Rutile. Indian Journal of Chemistry. 48(10), 1378-1382.

28. Ouzzine M., Romero-Anaya A.J., Lillo-Ródenas M.A., Linares-Solano A., 2013. Spherical Activated Carbon As An Enhanced Support For TiO_2/AC Photocatalysts. Carbon. 67, 104-118.

29. Slimen H., Houas A., Nogier J.P., 2011. Elaboration of Stable Anatase TiO_2 Through Activated Carbon Addition With High Photocatalytic Activity Under Visible Light. Journal of Photochemistry and Photobiology A: Chemistry. 221(1), 13-21.

30. Wang X., Liu Y., Hu Z., Chen Y., Liu W., Zhao G., 2009. Degradation Of Methyl Orange By Composite Photocatalysts Nano-Tio2 Immobilized On Activated Carbons Of Different Porosities. Journal of Hazardous Materials. 169(1-3), 1061-1067.

31. Nguyen N.V., Nguyen N.K.T., Phi H.N., 2011. Hydrothermal Synthesis Of Fe-Doped Tio2 Nanostructure Photocatalyst. Advances in Natural Sciences: Nanoscience and Nanotechnology. 2(3), 035014.

32. Peter Etape E., John Ngolui L., Foba-Tendo, J., Yufanyi, D., Victorine Namondo B., 2017. Synthesis And Characterization of Cuo, TiO_2, And Cuo-TiO_2 Mixed Oxide By A Modified Oxalate Route. Journal of Applied Chemistry. 2017(1), 1-10.

33. Avilés-García O., Espino-Valencia J., Romero-Romero R., Rico-Cerda J.L., Arroyo-Albiter M., Solís-Casados D.A., Natividad-Rangel R., 2018. Enhanced Photocatalytic Activity Of Titania By Co-Doping With Mo And W. Catalysts. 8(12), 631.

34. Bashiri R., Mohamed N.M, Kait C.F., Sufian S., 2015. Hydrogen Production From Water Photosplitting Using Cu/TiO_2 Nanoparticles: Effect of Hydrolysis Rate And Reaction Medium. International Journal of Hydrogen Energy. 40(18), 6021-6037.